Statistically optimized near field acoustic holography using an array of pressure-velocity probes[a)]

Finn Jacobsen[b)] and Virginie Jaud[c)]
Acoustic Technology, Ørsted-DTU, Technical University of Denmark, Building 352, Ørsteds Plads, DK-2800 Kgs. Lyngby, Denmark

(Received 1 September 2006; revised 15 December 2006; accepted 19 December 2006)

Statistically optimized near field acoustic holography (SONAH) differs from conventional near field acoustic holography (NAH) by avoiding spatial Fourier transforms; the processing is done directly in the spatial domain. The main advantage of SONAH compared with NAH is that the usual requirement of a measurement aperture that extends well beyond the source can be relaxed. Both NAH and SONAH are based on the assumption that all sources are on one side of the measurement plane whereas the other side is source free. An extension of the SONAH procedure based on measurement with a double layer array of pressure microphones has been suggested. The double layer technique makes it possible to distinguish between sources on the two sides of the array and thus suppress the influence of extraneous noise coming from the "wrong" side. It has also recently been demonstrated that there are significant advantages in NAH based on an array of acoustic particle velocity transducers (in a single layer) compared with NAH based on an array of pressure microphones. This investigation combines the two ideas and examines SONAH based on an array of pressure-velocity intensity probes through computer simulations as well as experimentally. [DOI: 10.1121/1.2434245]

PACS number(s): 43.60.Sx, 43.60.Pt, 43.20.Rz [EJS] Pages: 1550–1558

I. INTRODUCTION

Near field acoustic holography (NAH) is an experimental technique that makes it possible to reconstruct three-dimensional sound fields from measurements on two-dimensional surfaces. This can be extremely useful, and NAH is a well-established tool for visualizing and analyzing sound fields near sources of noise.[1,2] Conventional planar NAH is based on discrete spatial Fourier transforms of sound pressure data measured with a microphone array. However, to avoid serious truncation errors caused by the finite two-dimensional spatial transform ("leakage" in the wave number domain) the array must extend well beyond the source so that the sound pressure has decayed to an insignificant level near the edges of the array.[2]

Statistically optimized near field acoustic holography (SONAH) is an interesting variant of NAH developed a few years ago by Steiner and Hald.[3] It has the great advantage of avoiding spatial transforms and thus the mentioned truncation effects; therefore the measurement array can be smaller than the source.[3–5]

Both NAH and SONAH are usually based on measurement of the sound pressure. However, an acoustic particle velocity transducer has been available for some years,[6] and it has recently been demonstrated that NAH based on measurement of the normal component of the particle velocity is more accurate than pressure-based NAH.[7] The purpose of this paper is to examine whether there is a similar advantage in measuring the particle velocity with the SONAH procedure and, in particular, to examine whether one can combine predictions based on measurement of the sound pressure with predictions based on measurement of the normal component of the particle velocity and thereby be able to distinguish between sound coming from the two sides of the measurement plane in the same way as one can do that with a double layer array of pressure transducers.[8–10]

II. OUTLINE OF THEORY

A. SONAH based on measurement of the sound pressure

The following derivation is based on Hald.[4] In planar SONAH the "propagator" that transforms data from one plane to another is a transfer matrix that works directly on the measured data. Thus the sound pressure at an arbitrary position above the source, $\mathbf{r}=(x,y,z)$ (where $z>0$), is expressed as a weighted sum of sound pressures measured at N positions ($\mathbf{r}_{h,n}$) in the hologram plane ($z=z_h$),

$$p(\mathbf{r}) \simeq \sum_{n=1}^{N} c_n(\mathbf{r}) p(\mathbf{r}_{h,n}) = \mathbf{p}^T(\mathbf{r}_h)\mathbf{c}(\mathbf{r}), \tag{1}$$

where T indicates that the column vector $\mathbf{p}(\mathbf{r}_h)$ is transposed. The transfer vector $\mathbf{c}(\mathbf{r})$ does not depend on the sound field but only on positions. It is determined by requiring that an infinite set of propagating and evanescent elementary waves of the form

[a)]Portions of this work were presented in "Statistically optimised near field acoustic holography based on particle velocity measurements," Proceedings of the 13th International Congress on Sound and Vibration, Vienna, Austria, July 2006, and in "Statistically optimised near field acoustic holography with an array of pressure-velocity intensity probes," Proceedings of Inter-Noise 2006, Honolulu, HI, December 2006.

[b)]Author to whom correspondence should be addressed; electronic mail: fja@oersted.dtu.dk
[c)]Electronic mail: virginie.jaud@gmail.com

$$\Phi_m(\mathbf{r}) = e^{-j(k_{x,m}x+k_{y,m}y+k_{z,m}z)}, \quad m = 1,2,\ldots,M,\ M \to \infty, \tag{2}$$

where

$$k_{z,m} = \begin{cases} \sqrt{k^2 - k_{x,m}^2 - k_{y,m}^2} & \text{for } \sqrt{k_{x,m}^2 + k_{y,m}^2} \leqslant k \\ -j\sqrt{k_{x,m}^2 + k_{y,m}^2 - k^2} & \text{for } \sqrt{k_{x,m}^2 + k_{y,m}^2} > k \end{cases} \tag{3}$$

(with the $e^{j\omega t}$ sign convention) are projected from the measurement plane to the prediction plane [in other words, satisfy Eq. (1)] with optimal accuracy. As can be seen from Eq. (2) all the elementary waves have an amplitude of unity in the source plane, from which it follows that the transfer vector $\mathbf{c}(\mathbf{r})$ is optimized for a "white" wave number spectrum in this plane; hence the term "statistically optimal" near field acoustic holography.[3–5] In vector and matrix form,

$$\boldsymbol{\alpha}(\mathbf{r}) \simeq \mathbf{A}\mathbf{c}(\mathbf{r}), \tag{4}$$

where $\boldsymbol{\alpha}(\mathbf{r})$ is a column vector with M elements, $[\boldsymbol{\alpha}(\mathbf{r})]_m = \Phi_m(\mathbf{r})$, and $\mathbf{A}$ is an M by N matrix, $[\mathbf{A}]_{mn} = \Phi_m(\mathbf{r}_{h,n})$. Since $M > N$ Eq. (4) is overdetermined. The least-squares solution is

$$\mathbf{c}(\mathbf{r}) = (\mathbf{A}^H\mathbf{A} + \theta^2\mathbf{I})^{-1}\mathbf{A}^H\boldsymbol{\alpha}(\mathbf{r}), \tag{5}$$

where $\mathbf{I}$ is the identity matrix, θ is a regularization parameter, and the superscript H indicates the Hermitian transpose.[3–5] Note that $\mathbf{A}^H\mathbf{A}$ is an N by N matrix and $\mathbf{A}^H\boldsymbol{\alpha}(\mathbf{r})$ is a column vector with N elements. It now follows that the sound pressure in the prediction plane is

$$p(\mathbf{r}) = \mathbf{p}^T(\mathbf{r}_h)(\mathbf{A}^H\mathbf{A} + \theta^2\mathbf{I})^{-1}\mathbf{A}^H\boldsymbol{\alpha}(\mathbf{r}). \tag{6}$$

The normal component of the particle velocity in the prediction plane is obtained from Eq. (6) using Euler's equation of motion,

$$\begin{aligned} u_z(\mathbf{r}) &= \frac{-1}{j\omega\rho}\mathbf{p}^T(\mathbf{r}_h)(\mathbf{A}^H\mathbf{A} + \theta^2\mathbf{I})^{-1}\frac{\partial\mathbf{A}^H\boldsymbol{\alpha}(\mathbf{r})}{\partial z} \\ &= \mathbf{p}^T(\mathbf{r}_h)(\mathbf{A}^H\mathbf{A} + \theta^2\mathbf{I})^{-1}\mathbf{A}^H\boldsymbol{\beta}(\mathbf{r}), \end{aligned} \tag{7}$$

where the only quantity that is differentiated is the vector $\mathbf{A}^H\boldsymbol{\alpha}(\mathbf{r})$ since this is the only quantity that depends on z.

In practice it is desirable to estimate the sound pressure and the particle velocity not just at a single position $\mathbf{r}$ but in a grid of N points in a plane; thus the column vectors $\mathbf{A}^H\boldsymbol{\alpha}$ and $\mathbf{A}^H\boldsymbol{\beta}$ become N by N matrices, and the left-hand sides of Eqs. (6) and (7) become column vectors. When $M \to \infty$ the elements of $\mathbf{A}^H\mathbf{A}$, $\mathbf{A}^H\boldsymbol{\alpha}$, and $\mathbf{A}^H\boldsymbol{\beta}$ turn into integrals over k_x and k_y that can be evaluated numerically.[3–5] The infinite column vector $\boldsymbol{\alpha}(\mathbf{r})$ and the infinite matrix $\mathbf{A}$ are not determined at all.

B. SONAH based on measurement of the particle velocity

It is a fairly simple matter to extend the foregoing considerations to the case where the normal component of the particle velocity rather than the sound pressure is measured. For any of the elementary waves the pressure ratio $p(\mathbf{r})/p(\mathbf{r}_{h,n})$ is identical to the particle velocity ratio $u_z(\mathbf{r})/u_z(\mathbf{r}_{h,n})$, which leads to the conclusion that the transfer vector given by Eq. (5) also projects the normal component of the particle velocity from the measurement plane to the prediction plane. Thus

$$u_z(\mathbf{r}) = \mathbf{u}_z^T(\mathbf{r}_h)(\mathbf{A}^H\mathbf{A} + \theta^2\mathbf{I})^{-1}\mathbf{A}^H\boldsymbol{\alpha}(\mathbf{r}). \tag{8}$$

One can also predict the sound pressure from the measured normal component of the particle velocity, as follows:

$$\begin{aligned} p(\mathbf{r}) &= \mathbf{u}_z^T(\mathbf{r}_h)(\mathbf{A}^H\mathbf{A} + \theta^2\mathbf{I})^{-1}(-j\omega\rho)\int \mathbf{A}^H\boldsymbol{\alpha}(\mathbf{r})dz \\ &= \mathbf{u}_z^T(\mathbf{r}_h)(\mathbf{A}^H\mathbf{A} + \theta^2\mathbf{I})^{-1}\mathbf{A}^H\boldsymbol{\gamma}(\mathbf{r}), \end{aligned} \tag{9}$$

where the only quantity that is integrated is the vector $\mathbf{A}^H\boldsymbol{\alpha}(\mathbf{r})$ since this is the only quantity that depends on z.

Equations (8) and (9) can, of course, be extended from a single position to N positions in the prediction plane in the same way as Eqs. (6) and (7); and in the limit of $M \to \infty$ the elements of $\mathbf{A}^H\boldsymbol{\gamma}$ become integrals that can be evaluated numerically in the same way as the elements of $\mathbf{A}^H\mathbf{A}$, $\mathbf{A}^H\boldsymbol{\alpha}$, and $\mathbf{A}^H\boldsymbol{\beta}$. See the Appendix.

C. SONAH based on measurement of the pressure and the particle velocity

One cannot distinguish between sound coming from the two sides of the measurement plane if one measures only the sound pressure or the normal component of the particle velocity. However, if both quantities are measured then the fact that the particle velocity unlike the pressure is a vector component that changes its sign if the source is moved to a symmetrical position on the other side of the measurement plane makes it possible to separate the two contributions from each other. Thus the pressure generated by the primary source can be estimated as the average of a pressure- and a particle velocity-based estimate,

$$\begin{aligned} p(\mathbf{r}) = \tfrac{1}{2}(&\mathbf{p}^T(\mathbf{r}_h)(\mathbf{A}^H\mathbf{A} + \theta^2\mathbf{I})^{-1}\mathbf{A}^H\boldsymbol{\alpha}(\mathbf{r}) \\ &+ \mathbf{u}_z^T(\mathbf{r}_h)(\mathbf{A}^H\mathbf{A} + \theta^2\mathbf{I})^{-1}\mathbf{A}^H\boldsymbol{\gamma}(\mathbf{r})), \end{aligned} \tag{10}$$

and the particle velocity can be estimated in a similar way,

$$\begin{aligned} u_z(\mathbf{r}) = \tfrac{1}{2}(&\mathbf{u}_z^T(\mathbf{r}_h)(\mathbf{A}^H\mathbf{A} + \theta^2\mathbf{I})^{-1}\mathbf{A}^H\boldsymbol{\alpha}(\mathbf{r}) \\ &+ \mathbf{p}^T(\mathbf{r}_h)(\mathbf{A}^H\mathbf{A} + \theta^2\mathbf{I})^{-1}\mathbf{A}^H\boldsymbol{\beta}(\mathbf{r})). \end{aligned} \tag{11}$$

However, since the transfer matrices have been optimized for elementary waves coming from the source plane one should perhaps not expect the same accuracy in the general case where the disturbing noise is not coming from a source placed symmetrically. A future investigation will examine the influence of the wave number weighting.

In what follows this combination of estimates based on pressure and velocity is referred to as "the *p-u* method." In principle one could also determine the pressure and the particle velocity generated by the disturbing sources on the other side of the measurement plane by subtracting instead of adding the pressure- and particle velocity-based estimates.

III. A SIMULATION STUDY

To examine the performance of the methods described in the foregoing a simulation study has been carried out. Sev-

eral test cases were examined, including combinations of point sources and point driven simply supported vibrating panels mounted in infinite baffles without and with disturbing background noise from a monopole placed on the "wrong" side of the measurement plane. The structural sources were modeled by modal sums, and the radiated sound fields were calculated from numerical approximations to Rayleigh's first integral.[2] In all cases there were 8×8 sound pressure and particle velocity transducers in the simulated measurement array; the measurement plane was 6 cm from the source, the prediction plane was 3 cm from the source, and both planes had dimensions 21×21 cm corresponding to 3 cm between adjacent positions.

The recommended value of the regularization parameter θ is related to the signal-to-noise ratio,[3,4] which, however, can be difficult to estimate.[11] The results presented in what follows are based on an alternative regularization technique, the generalized cross validation method.[11,12] This method (which is similar to the technique described in Ref. 5) has the advantage that no *a priori* knowledge about the signal-to-noise ratio of the data is needed.

A. Simple SONAH with ideal transducers

Figure 1 shows a typical set of results from the first test case, a baffled 5 mm steel panel of size 21×21 cm, that is, of the same size as the measurement plane, driven at 500 Hz by a point force near a corner. (Rayleigh's integral was approximated by 32×32 point sources on the baffle.) Figure 1(a) compares the pressure predicted from the pressure and from the velocity with the "true" pressure along a diagonal, and Fig. 1(b) compares the velocity predicted from the velocity and from the pressure with the "true" velocity (note that the velocity reference is 50 nm/s). Inspection shows that the best results are obtained if the pressure is predicted from the pressure and the velocity is predicted from the velocity.

B. The influence of amplitude and phase mismatch

Figure 2 demonstrates the influence of amplitude mismatch on SONAH predictions of the sound field generated by a baffled 5 mm steel plate of size 1×1 m, driven by a point force near a corner. (In this case Rayleigh's integral was approximated by 64×64 point sources on the baffle.) Figure 2 shows five outcomes of a stochastic experiment where independent random amplitude mismatch evenly distributed between ±0.5 dB has been introduced in each of the "measured" pressure and velocity signals. Not surprisingly, such amplitude mismatch has a negative influence on the performance of the SONAH procedure. By far the most serious effect occurs when the particle velocity is predicted from pressure data, and pressure-to-pressure and particle velocity-to-particle velocity predictions are the least affected. These observations agree with observations from conventional NAH simulations.[7]

Very similar results have been obtained with phase mismatch (not shown).

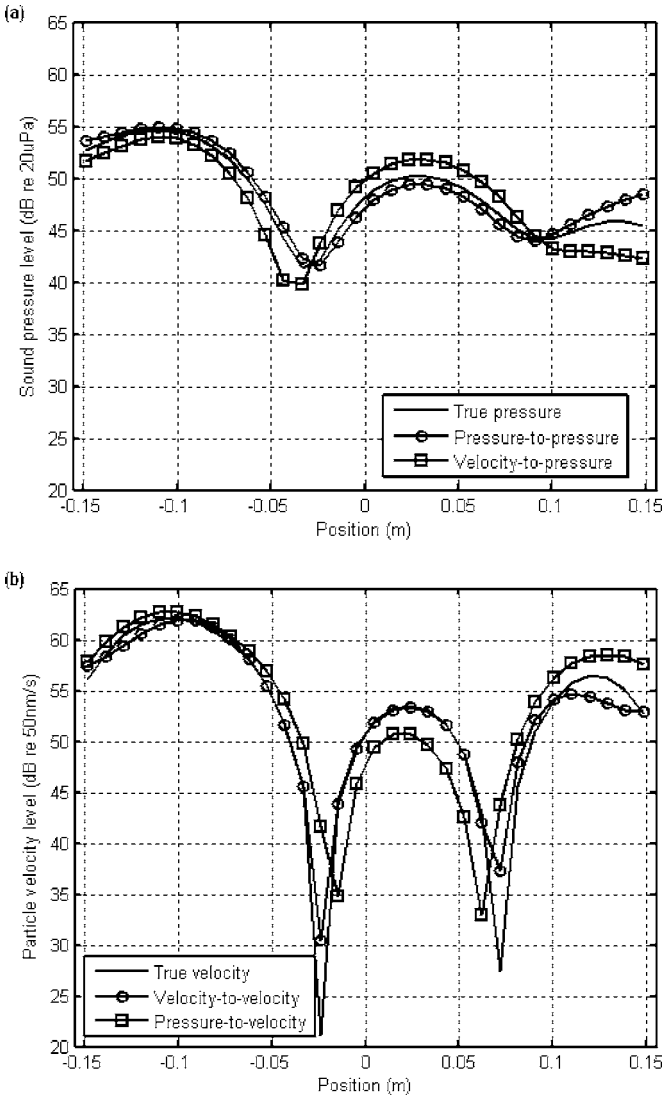

FIG. 1. Small panel in a baffle driven at 500 Hz. (a) "True" and predicted sound pressure and (b) true and predicted particle velocity in a diagonal across the prediction plane.

C. The pressure-velocity method

The *p-u* method based on Eqs. (10) and (11) has been examined with combinations of simple sources disturbed by other simple sources, with vibrating panels disturbed by simple sources, and with an infinite vibrating plate disturbed by simple sources.

Figures 3 and 4 show the results of a test case with two interfering plane waves propagating in the *yz* plane at angles of ±40° from the normal to the *z* plane at 3 kHz disturbed by two monopoles on the "wrong" side of the measurement plane, located at (0, 0, 16) and $(-12,-2,16)$, respectively [coordinates in centimeters, and (0, 0, 6) being the coordinate of the center of the measurement plane]. The two interfering plane waves might conceivably be generated by two supersonic bending waves traveling in opposite directions on an infinite plate at $z=0$ (or in any other parallel plane on the "right" side of the measurement plane). This is an extreme test case since (i) the primary source is infinite, so the measurement array is infinitely smaller than the source, and (ii) the wave number spectrum of the primary source consists of

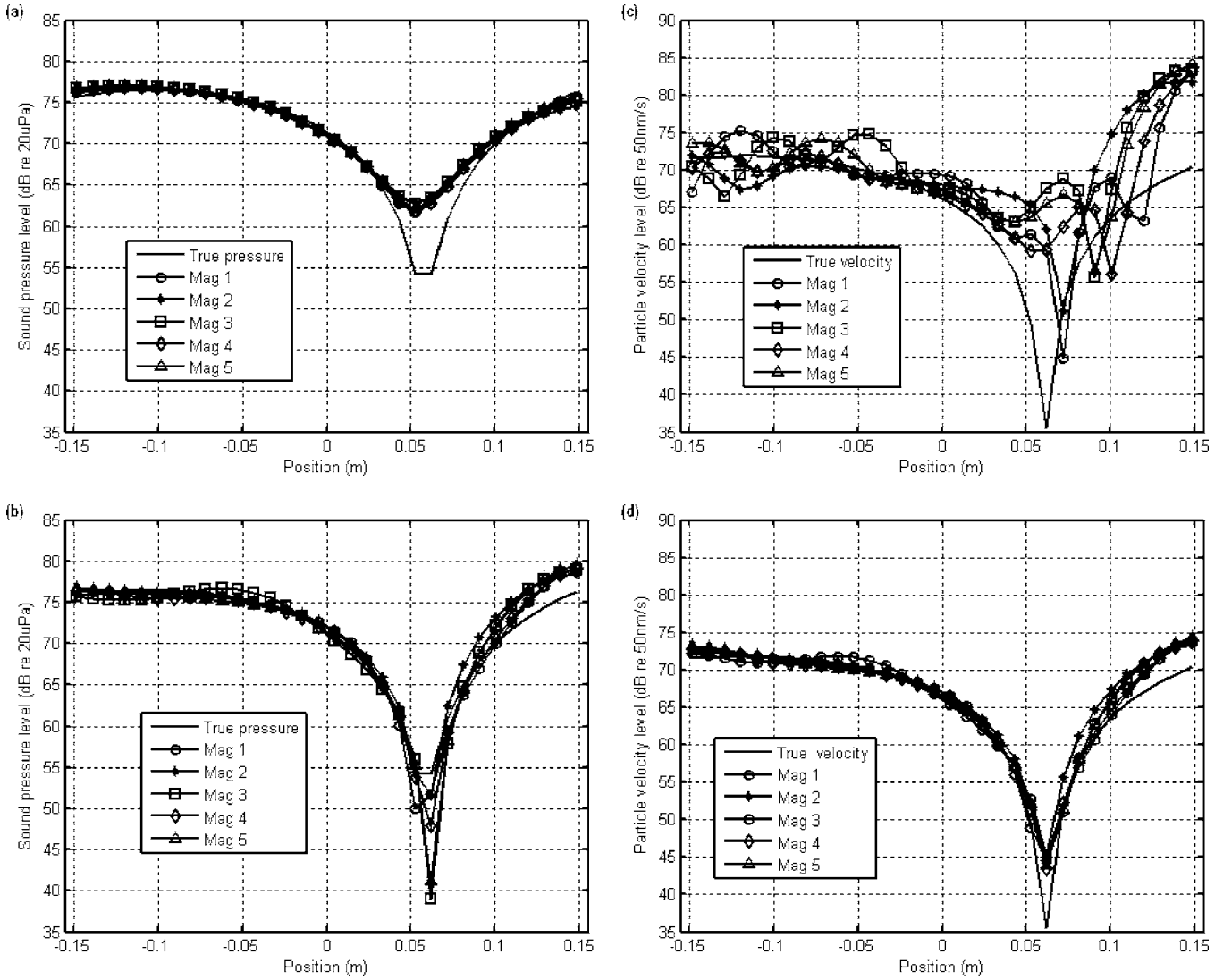

FIG. 2. The influence of transducer amplitude mismatch on predictions near a large panel driven at 600 Hz. (a) Pressure predicted from pressure; (b) pressure predicted from particle velocity; (c) particle velocity predicted from pressure; (d) particle velocity predicted from particle velocity. All quantities are shown in a diagonal across the prediction plane.

two delta functions and is thus very far from "white." As can be seen in Fig. 3 the two monopoles generate a sound pressure level comparable to the level of the two plane waves in the prediction plane. Figure 4 demonstrates that predictions based only on pressure or velocity are severely contaminated by the disturbing sources whereas the *p-u* method performs reasonably well. The reason for the poor performance of predictions based on either the pressure or the particle velocity is, of course, that the predicted sound field generated by the disturbing monopoles will be added to the predicted primary sound field (in pressure-based predictions) or subtracted from it (in velocity-based predictions), since these predictions are based on the assumption of a source-free region on the "wrong" side of the measurement plane. Similar simulations (not shown here, but presented in Ref. 13) have demonstrated that pressure-to-pressure and particle velocity-to-particle velocity predictions in the absence of extraneous noise are more accurate than the *p-u* method. All in all it can be concluded that (i) SONAH can indeed cope with sources that are larger than the measurement array—even infinitely

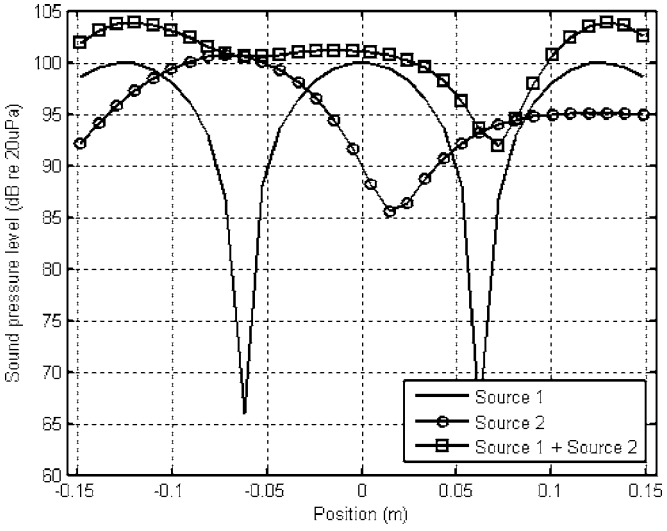

FIG. 3. Sound pressure level in a diagonal across the prediction plane generated by two interfering plane waves and two monopoles on the "wrong" side of the measurement plane.

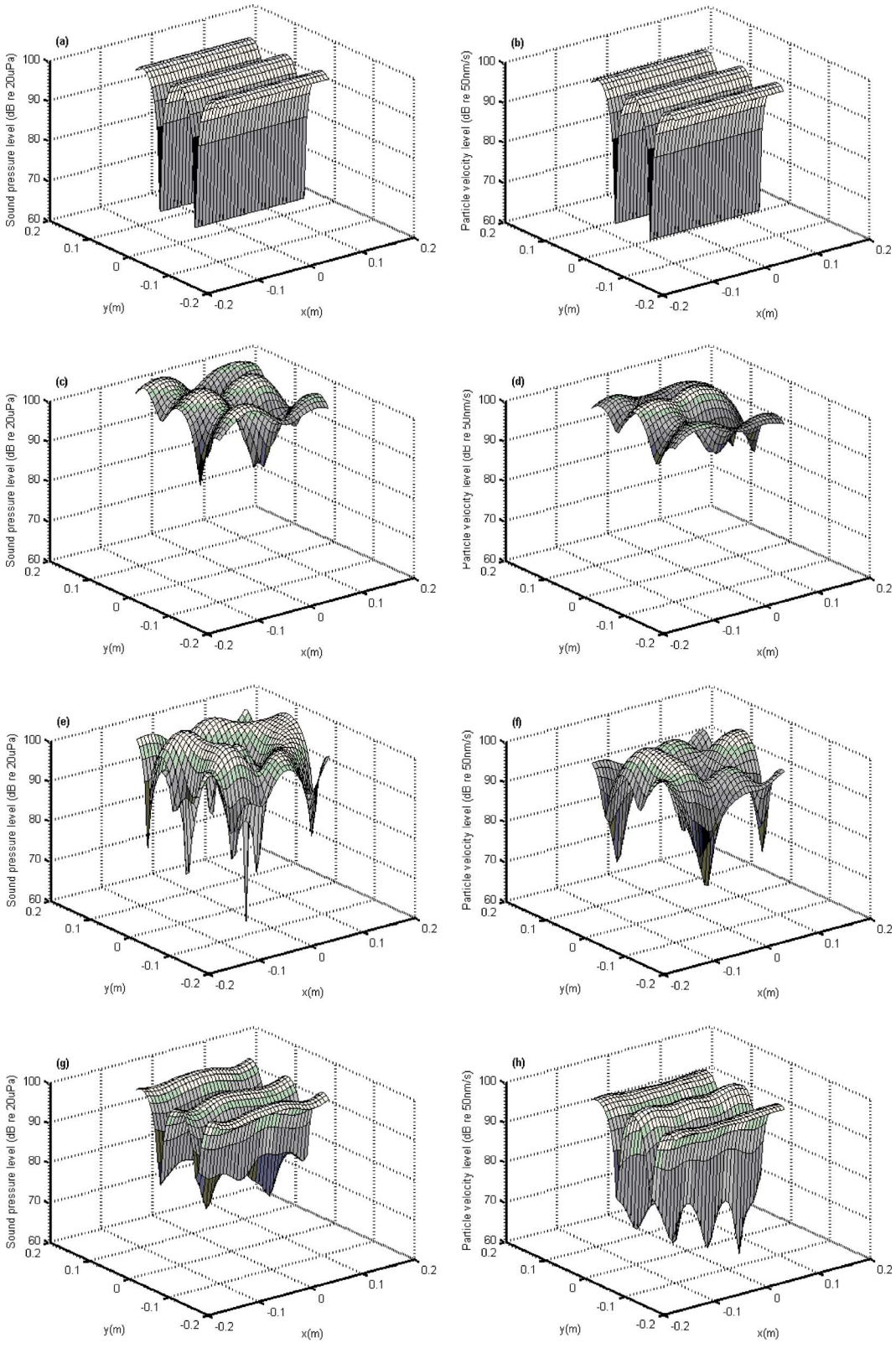

FIG. 4. Two interfering plane waves disturbed by two monopoles on the wrong side of the measurement plane. Left column (a, c, e, g), sound pressure; right column (b, d, f, h), particle velocity; top row, true (undisturbed) sound field; second row, predictions from the sound pressure; third row, predictions from the particle velocity; bottom row, predictions with the *p-u* method.

larger; (ii) SONAH gives good predictions even when the wave number spectrum in the source plane is extremely far from "white"; (iii) in the absence of disturbing noise, pressure-to-pressure and particle velocity-to-particle velocity predictions work better than predicting one quantity from the other; and (iv) the *p-u* method copes successfully with disturbing noise.

Figure 5 shows a typical example of the results of the

SONAH procedures based on Eqs. (6)–(11) when the sound field generated by the large baffled panel is disturbed by sound from a monopole on the other side of the measurement plane. The monopole, located at (0, 0, 16), generates a sound pressure level in the prediction plane that is comparable to the level generated by the primary source. It is apparent that *p-u* method works fairly well whereas predictions based either on the pressure or on the particle velocity are seriously affected by the disturbing sources. The same source configuration has been examined with a lower level of extraneous noise, with a higher level, and with a much higher level. Not surprisingly the results (not shown) demonstrate that the advantage of the *p-u* method vanishes if the disturbing signal is low enough. They also show that the method can, of course, only cope with disturbing noise within limits; when the level of the noise is more than 20 dB higher than the primary noise the method no longer works.

It should be mentioned that the image source resulting from reflections in the source plane has been ignored in determining the results shown in Fig. 5. Adding such a source increases the error of the *p-u* method. Unfortunately there is no way of eliminating the sound field produced by image sources caused by reflections in the primary source since they are placed on the "right" side of the measurement plane; this is simply a fundamental limitation of any *p-u* or double layer technique.

IV. EXPERIMENTAL RESULTS

Some experiments have been carried out in DTU's large anechoic room. Three different sources were used, a "monopole" (a Brüel & Kjær (B&K) 4299 "Volume Velocity Source," which is a tube with a built-in sound intensity probe connected to a B&K 4295 "OmniSource" loudspeaker[14]), a "monopole on a sphere" (a device consisting of a hollow rigid sphere with a small hole driven by an internal loudspeaker, developed for calibrating *p-u* sound intensity probes[15]), and a model of a helicopter gearbox driven by an internal B&K 4809 electrodynamic exciter. The monopole on a sphere and the gearbox are shown in Figs. 6(a) and 6(b). The sound pressure and the particle velocity were measured at 6×6 points in two planes of 25×25 cm using a single $\frac{1}{2}$ in. *p-u* sound intensity probe produced by Microflown.[6] The transducer, which was calibrated as described in Ref. 15, was moved manually over the two measurement planes using a "manual robot," shown in Fig. 6(b). The two measurement planes were 6 and 3 cm from the nearest part of the source (all of which had a curved surface); the measurement plane near the source served the purpose of providing the true sound pressure and particle velocity in the prediction plane. A B&K "PULSE" analyzer in 1/12 octave mode was used for measuring the frequency responses between each of the two output signals from the *p-u* probe and the signal driving the source under test.

Figure 7 shows an example of results obtained with the gearbox. In this case there was no noise from the "wrong" side of the measurement plane, and therefore there is no advantage in the *p-u* method; accordingly pressure-to-pressure and velocity-to-velocity predictions are slightly better than the *p-u* method.

Figure 8 shows results determined with the monopole as the primary source and the monopole on a sphere as disturbing source on the other side of the measurement plane. [The monopole was located at $(-5.5,9,0)$, and the monopole on a sphere was located with the hole at (3.5, 1.5, 23) and the sphere behind.] Figure 8(a) shows the sound pressure levels generated by the two sources in the prediction plane, Fig. 8(b) shows the global relative error of the sound pressure, Fig. 8(c) shows the global relative error of the particle velocity, and Fig. 8(d) shows the global relative error of the sound intensity. (The global relative error of, say, the sound pressure is defined as the ratio of the sum of the absolute values of all local deviations between the predicted and the true pressure to the sum of the absolute values of the local true pressure.[5]) The sound intensity has been determined in four different ways, from the pressure, from the particle ve-

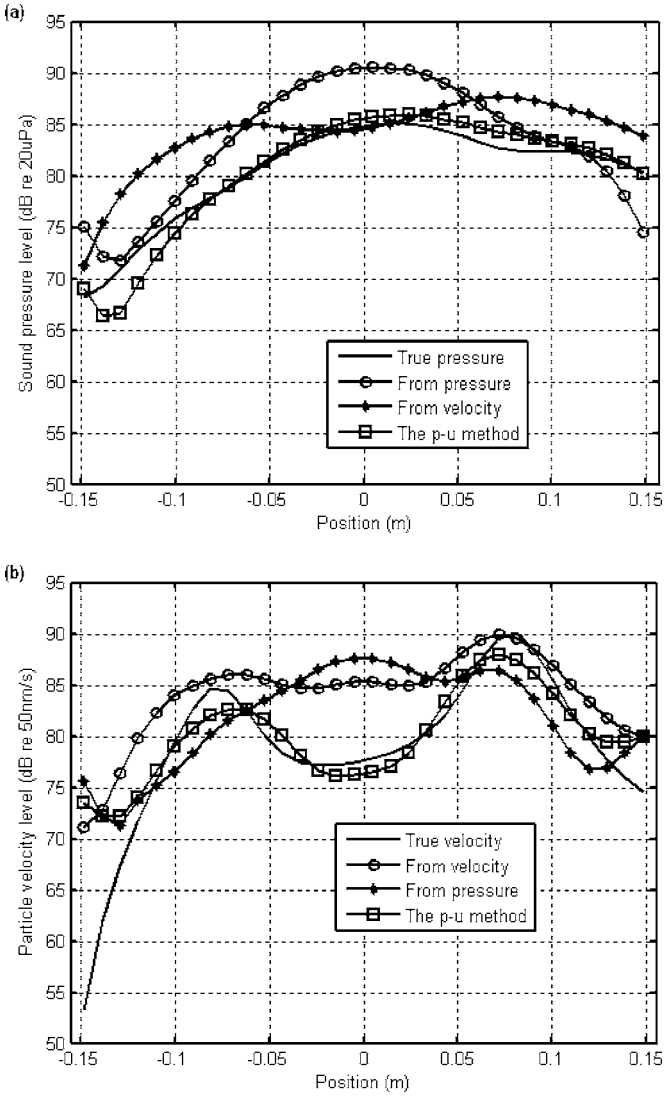

FIG. 5. Large panel driven at 1 kHz and disturbed by a monopole on the wrong side of the measurement plane. True (undisturbed) and predicted sound pressure (a) and true (undisturbed) and predicted particle velocity (b) in a diagonal across the prediction plane.

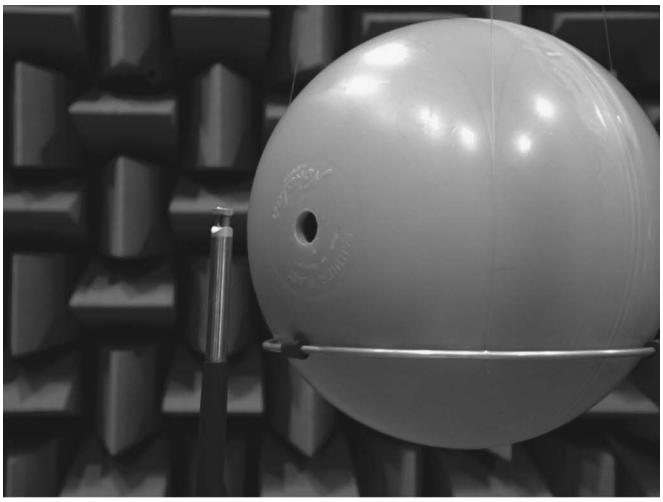

(a)

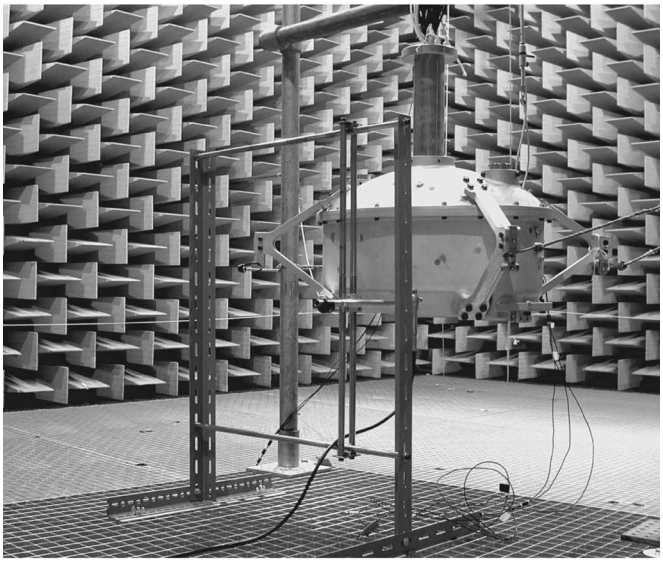

(b)

FIG. 6. Two sources in DTU's anechoic room, (a) the "monopole on a sphere" with the Microflown *p-u* intensity probe, and (b) the gearbox model driven by an internal exciter and the "manual robot" with the *p-u* probe.

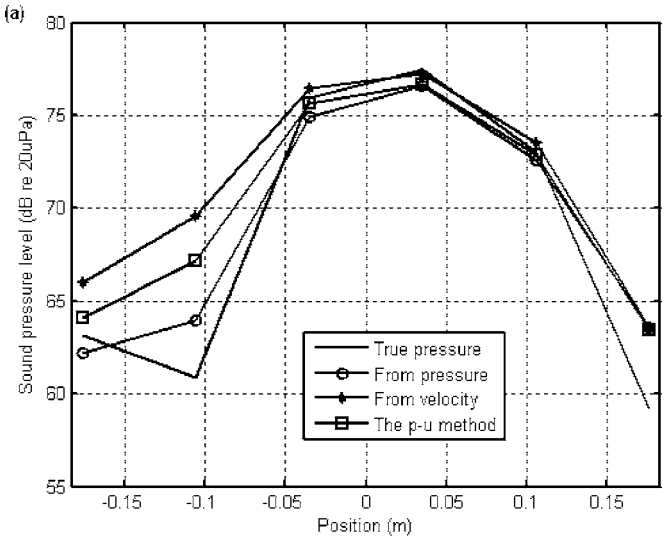

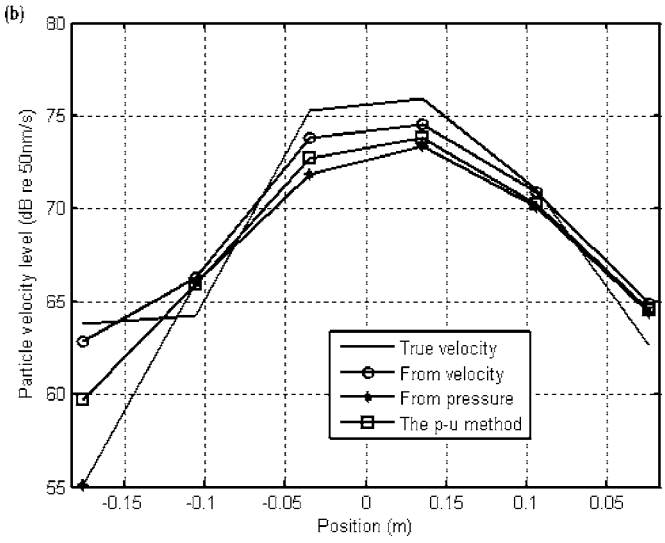

FIG. 7. Gearbox driven at 1 kHz. (a) True and predicted sound pressure, and (b) true and predicted particle velocity in a diagonal across the prediction plane.

locity, from the pressure determined from the pressure combined with the particle velocity determined from the particle velocity, and from pressure and particle velocity where both quantities have been determined from both quantities using the *p-u* method. Similar measurements (not shown) have been carried out with a lower level of the disturbing noise, and with a higher level. As expected the *p-u* method performs better than any other method when the signal-to-noise ratio is poor; otherwise the best solution is to predict the pressure from the pressure and the particle velocity from the particle velocity. However, if the disturbing noise level is much higher than the level generated by the source under test the *p-u* method breaks down.

V. DISCUSSION

A recent investigation of conventional NAH concluded that the accuracy of pressure-to-pressure predictions is comparable to the accuracy of velocity-to-velocity predictions, whereas the accuracy of velocity-to-pressure predictions is far better than the accuracy of pressure-to-velocity predictions.[7] It was also concluded that transducer mismatch has a significantly more serious influence on pressure-to-velocity predictions than on velocity-to-pressure predictions. In both cases the explanation was that the wave number ratio that occurs in the propagator when the pressure is predicted from the particle velocity in an inverse problem reduces high spatial frequencies associated with evanescent modes, whereas the reciprocal wave number ratio, which occurs when the particle velocity is predicted from the pressure, amplifies them.[7] The tendencies observed with SONAH predictions are similar; on the whole velocity-to-pressure predictions perform better than pressure-to-velocity predictions, in particular if the transducers are not perfectly matched. The explanation is undoubtedly the same as with NAH; although transforms to the wave number domain are avoided, high spatial frequencies are nevertheless reduced in the former case and amplified in the latter case. An additional advantage

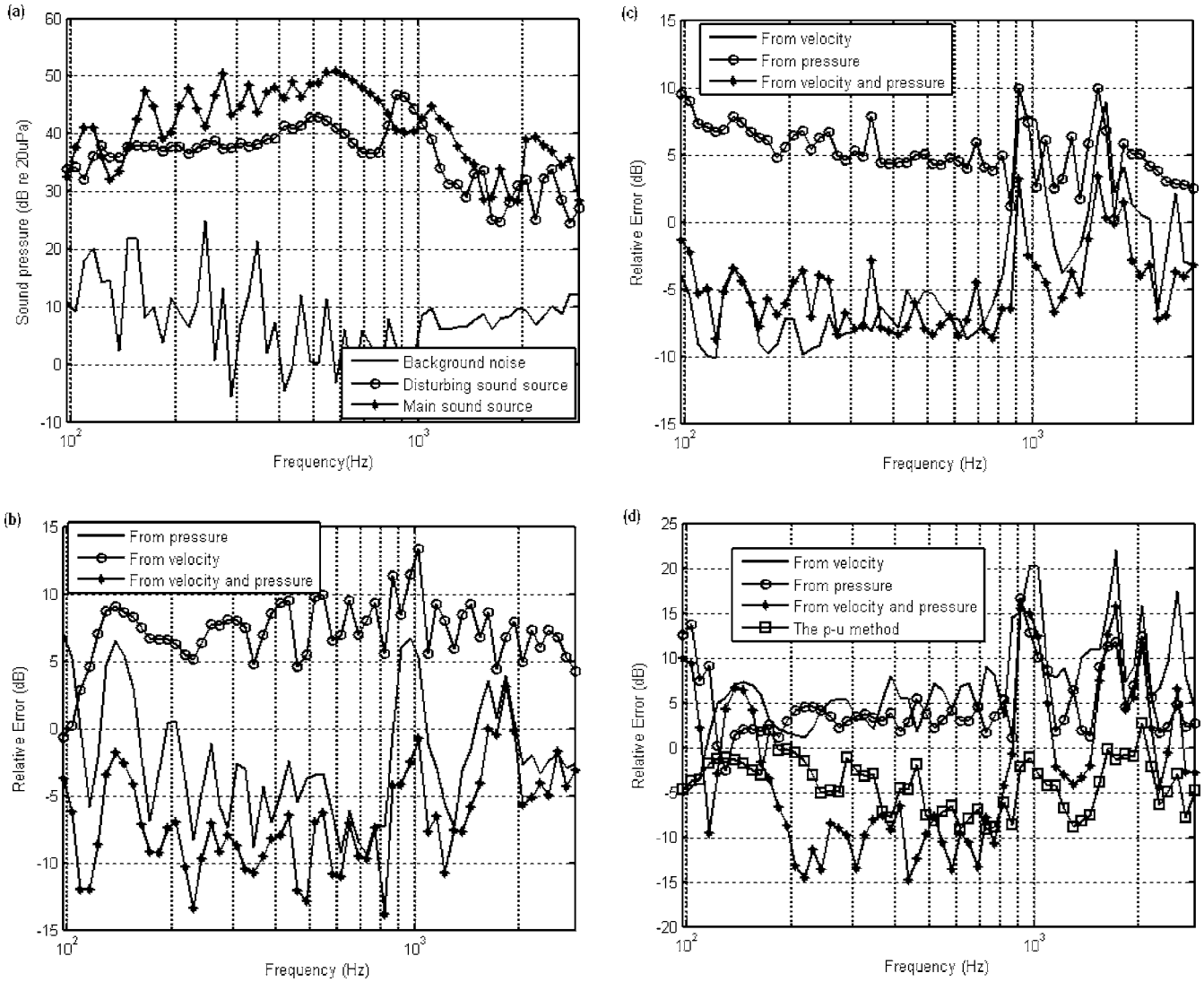

FIG. 8. Results obtained with the monopole disturbed by the monopole on a sphere. (a) Sound pressure level generated by the two sources at the center of the prediction plane; (b) relative error of predicted sound pressure, (c) particle velocity, and (d) sound intensity.

of particle velocity-based conventional NAH is that the normal component of the particle velocity because of the necessary, large measurement plane decreases faster toward the edges of the plane than the pressure does, which reduces spatial windowing effects.[7] This effect is not relevant with the SONAH procedure.

VI. CONCLUSIONS

Statistically optimized near field acoustic holography has usually been based on measurement of the sound pressure in a plane, but may as well be based on measurement of the normal component of the particle velocity. A simulation study has shown and experimental results have confirmed that SONAH with advantage can be based on measurement of both quantities, in particular if the transducers are less than perfectly matched, since it in general is better to predict the sound pressure from the sound pressure and the particle velocity from the particle velocity than to predict either quantity from the other quantity. Measuring both sound pressure and particle velocity has the additional advantage that it makes it possible—within limits—to reduce the influence of sound coming from the "wrong" side of the measurement array. In this case both the pressure and the particle velocity should be determined from both quantities.

ACKNOWLEDGMENT

The authors would like to thank Microflown for lending us a *p-u* sound intensity probe.

APPENDIX

The elements of the auto- and cross-correlation matrices $\mathbf{A}^H\mathbf{A}$, $\mathbf{A}^H\boldsymbol{\alpha}$, and $\mathbf{A}^H\boldsymbol{\beta}$ can be determined numerically as described in Ref. 4. This Appendix closely follows the derivation in Ref. 4 and describes how to calculate the elements of $\mathbf{A}^H\boldsymbol{\gamma}$.

In the limit of $M \to \infty$,

$$[\mathbf{A}^H \boldsymbol{\gamma}(\mathbf{r})]_n = \sum_m^M \Phi_m^*(\mathbf{r}_{h,n}) \rho c \frac{k}{k_z} \Phi_m(\mathbf{r}) \to \frac{\rho c}{\pi k} \int_{-\infty}^{\infty} \int_{-\infty}^{\infty} \frac{e^{j(k_x x_{h,n} + k_y y_{h,n} + k_z^* z_h)} e^{-j(k_x x + k_y y + k_z z)}}{k_z} \times dk_x dk_y. \tag{A1}$$

Changing to polar coordinates $[(k_x, k_y) = (K \cos \phi, K \sin \phi)]$ and introducing the function

$$w(K) = \frac{e^{j(k_z^* z_h - k_z z)}}{k_z} = \begin{cases} \dfrac{e^{-j\sqrt{k^2 - K^2}(z - z_h)}}{\sqrt{k^2 - K^2}} & \text{if } K^2 \leqslant k^2 \\ \dfrac{e^{-\sqrt{K^2 - k^2}(z + z_h)}}{-j\sqrt{K^2 - k^2}} & \text{if } K^2 > k^2 \end{cases} \tag{A2}$$

[cf. Eq. (3)], gives

$$\begin{aligned} [\mathbf{A}^H \boldsymbol{\gamma}(\mathbf{r})]_n &\to \frac{\rho c}{\pi k} \int_0^{\infty} \int_0^{2\pi} w(K) \times e^{-jK((x - x_{h,n})\cos\phi + (y - y_{h,n})\sin\phi)} K d\phi dK \\ &= \frac{\rho c}{\pi k} \int_0^{\infty} \int_0^{2\pi} w(K) \cos(K R_n \cos\phi) K d\phi dK \\ &= \frac{2\rho c}{k} \int_0^{k} \frac{e^{-j\sqrt{k^2 - K^2}(z - z_h)}}{\sqrt{k^2 - K^2}} J_0(K R_n) K dK \\ &\quad + \frac{j2\rho c}{k} \int_k^{\infty} \frac{e^{-\sqrt{K^2 - k^2}(z + z_h)}}{\sqrt{K^2 - k^2}} J_0(K R_n) K dK \\ &= 2\rho c \int_0^{\pi/2} e^{-jk\cos\theta(z - z_h)} J_0(k R_n \sin\theta) \sin\theta d\theta \\ &\quad + \frac{j2\rho c}{k(z + z_h)} \int_0^{\infty} J_0\left(k R_n \sqrt{1 + \frac{t^2}{k^2 (z + z_h)^2}}\right) e^{-t} dt, \end{aligned} \tag{A3}$$

where

$$K = k \sin\theta, \tag{A4}$$

$$R_n = \sqrt{(x_{h,n} - x)^2 + (y_{h,n} - y)^2}, \tag{A5}$$

and

$$t = \sqrt{K^2 - k^2}(z + z_h). \tag{A6}$$

The two integrals of Eq. (A3) are finally evaluated using Gauss and Gauss-Laguerre quadrature, respectively.

[1] J. D. Maynard, E. G. Williams, and Y. Lee, "Nearfield acoustic holography. I. Theory of generalized holography and the development of NAH," J. Acoust. Soc. Am. **78**, 1395–1413 (1985).

[2] E. G. Williams, *Fourier Acoustics—Sound Radiation and Nearfield Acoustical Holography* (Academic, San Diego, 1999).

[3] R. Steiner and J. Hald, "Near-field acoustical holography without the errors and limitations caused by the use of spatial DFT," Int. J. Acoust. Vib. **6**, 83–89 (2001).

[4] J. Hald, "Patch near-field acoustical holography using a new statistically optimal method," *Proceedings of Inter-Noise 2003*, Jeju Island, Korea, pp. 2203–2210.

[5] Y. T. Cho, J. S. Bolton, and J. Hald, "Source visualization by using statistically optimized nearfield acoustical holography in cylindrical coordinates," J. Acoust. Soc. Am. **118**, 2355–2364 (2005).

[6] R. Raangs, W. F. Druyvesteyn, and H.-E. de Bree, "A low-cost intensity probe," J. Audio Eng. Soc. **51**, 344–357 (2003).

[7] F. Jacobsen and Y. Liu, "Near field acoustic holography with particle velocity transducers," J. Acoust. Soc. Am. **118**, 3139–3144 (2005).

[8] M. Tamura, "Spatial Fourier transform method of measuring transmission coefficients at oblique incidence. I: Theory and numerical examples," J. Acoust. Soc. Am. **88**, 2259–2264 (1990).

[9] F. Yu, J. Chen, C. Bi, W. Li, and X. Chen, "Experimental investigation of sound field separation technique with double holographic planes," Chin. J. Acoust. **24**, 111–118 (2005).

[10] J. Hald, "Patch holography in cabin environments using a two-layer handheld array with an extended SONAH algorithm," *Proceedings of Euronoise 2006*, Tampere, Finland.

[11] J. Gomes, "Comparing parameter choice methods for the regularization in the SONAH algorithm," *Proceedings of Euronoise 2006*, Tampere, Finland.

[12] P. C. Hansen, *Rank-Deficient and Discrete Ill-Posed Problems: Numerical Aspects of Linear Inversion* (SIAM, Philadelphia, 1997).

[13] F. Jacobsen and V. Jaud, "Statistically optimized near field acoustic holography based on particle velocity measurements," *Proceedings of the 13th International Congress on Sound and Vibration*, Vienna, Austria, 2006.

[14] S. Gade, N. Møller, J. Hald, and J. Alkestrup, "The use of volume velocity source in transfer measurements," *Proceedings of Inter-Noise 2004*, Prague, Czech Republic.

[15] F. Jacobsen and V. Jaud, "A note on the calibration of pressure-velocity sound intensity probes," J. Acoust. Soc. Am. **120**, 830–837 (2006).